BIOCHEMISTRY
including biophysical chemistry & molecular biology

Article

pubs.acs.org/biochemistry

Conformational Analysis of the Frog Skin Peptide, Plasticin-L1, and Its Effects on Production of Proinflammatory Cytokines by Macrophages

Mariano A. Scorciapino,*[,†,‡] Giorgia Manzo,[†] Andrea C. Rinaldi,[§] Roberta Sanna,[†] Mariano Casu,[†] Jelena M. Pantic,[⊥] Miodrag L. Lukic,[⊥] and J. Michael Conlon[∥]

[†]Department of Chemical and Geological Sciences, University of Cagliari, Monserrato, Cagliari I-09042, Italy

[‡]Istituto Officina dei Materiali del Consiglio Nazionale delle Ricerche (IOM-CNR) UOS, Cagliari 09042, Italy

[§]Department of Biomedical Sciences, University of Cagliari, Monserrato, Cagliari I-09042, Italy

[⊥]Center for Molecular Medicine, University of Kragujevac, Kragujevac 34000, Serbia

[∥]Department of Biochemistry, United Arab Emirates University, Al Ain, United Arab Emirates

Supporting Information

ABSTRACT: Plasticin-L1 (GLVNGLLSSVLGGGQGGGG-LLGGIL) is a conformationally flexible glycine/leucine-rich peptide originally isolated from norepinephrine-stimulated skin secretions of the South-American Santa Fe frog *Leptodactylus laticeps* (Leptodactylidae). A nuclear magnetic resonance/molecular dynamics characterization of plasticin-L1 in the presence of dodecylphosphocholine (DPC) and DPC/sodium dodecylsulphate micelles as membrane-mimetic models showed that the peptide has affinity for both neutral and anionic membranes. The peptide adopts a stable helical conformation at the N-terminal region and a more disordered helix at the C-terminal region, separated by an unstructured loop wherein the highest number of glycines is localized. In both micelle environments, plasticin-L1 slowly inserts between the detergent head groups but always remains localized at the micelle/water interface. Plasticin-L1 lacks direct antimicrobial activity but stimulates cytokine production by macrophages. Incubation with plasticin-L1 (20 μg/mL) significantly ($P < 0.05$) increased the production of the proinflammatory cytokines IL-1β, IL-12, IL-23, and TNF-α from unstimulated peritoneal macrophages from both C57BL/6 and BALB/C mice. The peptide also increased IL-6 production by unstimulated ($P < 0.01$) and lipopolysaccharide-stimulated ($P < 0.01$) macrophages, whereas the effects on production of the anti-inflammatory cytokine IL-10 were not significant. These findings suggest that plasticin-L1 may play an immunomodulatory role in vivo by stimulating cytokine production from frog skin macrophages in response to microbial pathogens. This peptide may represent a template for the design of peptides with therapeutic applications as immunostimulatory agents.

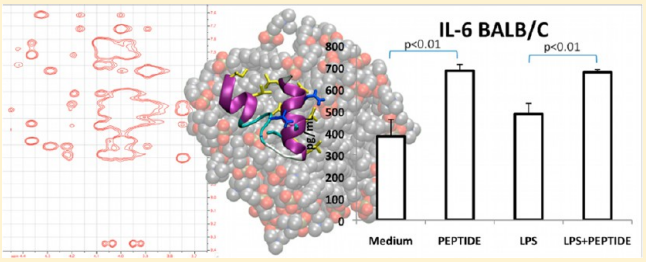

There is an urgent need for new types of antimicrobial agents at a time when we are witnessing an increasing incidence of infections caused by multidrug-resistant pathogenic bacteria and a dwindling supply of conventional antibiotics available to combat these infections.[1] The skins of anurans (frogs and toads) contain an important array of biologically active peptides, which play a role in several physiological processes.[2] In particular, vast numbers of such compounds have been isolated from skin secretions of many anuran species that display broad-spectrum antibacterial and antifungal activities and represent a key component of the animal's system of innate immunity.[3−5] The primary mode of action of the frog skin antimicrobial peptides involves nonspecific interaction with, and damage to, the cell membrane of the invading pathogens, and development of resistance to these agents occurs at much lower rates than those for conventional antibiotics.[6] The peptides show potential for development into therapeutically valuable anti-infective agents, either through their direct antimicrobial activity or through modulation and stimulation of the host's innate immune response.[7,8]

Plasticin-L1 (GLVNGLLSSVLGGGQGGGGLLGGIL) is a 25 amino-acid-residue glycine/leucine-rich peptide originally isolated from norepinephrine-stimulated skin secretions of the South-American Santa Fe frog *Leptodactylus laticeps* (Leptodactylidae).[9] Plasticin-L1 is a member of a structurally related family of gene-encoded, membrane-active host defense peptides that were first identified in the skins of phyllomedusid frogs from the family Hylidae.[10,11] The plasticins may be divided into two classes on the basis of their cytolytic activities. The strongly cationic peptides (plasticin-B1 and -S1), which contain several

Received: June 26, 2013
Revised: September 11, 2013
Published: September 27, 2013

dx.doi.org/10.1021/bi4008287 | *Biochemistry* 2013, 52, 7231−7241

lysine residues, show a potent broad spectrum antimicrobial activity and lyse erythrocytes, whereas the weakly cationic or neutral plasticins (plasticin-A1, -C1, -C2, and -DA1) are hemolytic only.[10,12] The biological role of plasticin-L1 is unknown. The peptide does not inhibit the growth of either *Escherichia coli* or *Staphylococcus aureus* at concentrations up to 500 μM and, unlike the other neutral plasticins from phyllomedusid frogs, lacks hemolytic activity. Plasticin-L1 stimulates the rate of release of insulin from rat clonal BRIN-BD11 cells without loss of integrity of the plasma membrane, but it seems improbable that this observation has physiological significance.[9] In common with other members of the plasticin family, the conformation of plasticin-L1 is markedly solvent dependent with the peptide displaying a random coil conformation in water, a β-sheet structure in methanol, and an α-helical folding in 50% trifluoroethanol (TFE)−water.[9]

The present study uses nuclear magnetic resonance (NMR) and molecular dynamics (MD) to determine the conformation of plasticin-L1 in membrane-mimetic environments represented by neutral dodecylphosphocholine (DPC) micelles, a model of the zwitterionic eukaryotic plasma membrane, and anionic mixed DPC/sodium dodecylsulphate (SDS) micelles, a model of the negatively charged prokaryotic cell membrane. The study also investigates the effect of plasticin-L1 on the release of pro- and anti-inflammatory cytokines from mouse peritoneal macrophages and identifies a possible in vivo immunomodulatory role for the peptide.

MATERIALS AND METHODS

Materials. Synthetic plasticin-L1 (GLVNGLLSSVLGGG-QGGGGLLGGIL) was purchased from AnaSpec (Fremont, CA, USA) at a purity of 98%. All the perdeuterated solvents employed, such as methanol-d_4, chloroform-d, trifluoroethanol-d_6, and dimethyl sulfoxide-d_6 were purchased from Sigma-Aldrich (St. Louis, MO, USA) with a purity ≥99%. Perdeuterated SDS-d_{25} and DPC-d_{38}, as well as 3-(trimethylsilyl)-2,2′,3,3′-tetradeuteropropionic acid (TSP-d_4), were purchased from Cambridge Isotope Laboratories (Andover, MA, USA) with a purity of 98%. All other chemicals were supplied by Sigma-Aldrich.

Hydropathicity Analysis. Hydropathicity values have been calculated with the ProtScale tool[13] available on the ExPaSy server (http://expasy.org/) The method of Kyte and Doolittle[14] was applied with a window size of three residues and a relative weight of the window edges of 30% compared to the weight of the window center.

Nuclear Magnetic Resonance. Studies were carried out in two different buffered (phosphate buffer 10 mM, pH 7.4) micellar systems: pure DPC micelles and 1:1 mol/mol DPC/SDS micelles. The employment of the latter model is validated by a recent study in which DPC and SDS were shown to be synergic in the formation of mixed micelles.[15] Plasticin-L1 was dissolved in 700 μL of buffered micelle solution at a final concentration of ∼2 mM. The peptide/detergent molar ratio was 1:100. Spectra were acquired with a Unity Inova 500NB high-resolution spectrometer (Agilent Technologies, Santa Clara, CA, USA) operating at a ^{1}H frequency of 500 MHz, equipped with a high-field indirect detection probe. Experiments were carried out at 300 K. The chemical shift scale of either ^{1}H and ^{13}C was referenced to the methyl signal of TSP. ^{1}H spectra were acquired using a 6.7 μs pulse (90°), 1.5 s delay time, 2 s acquisition time, and a spectral width of 6.5 kHz. Suppression of the water signal was achieved through application of the WET sequence,[16,17] which uses a combination of shaped selective excitation (uburp shape was centered at water resonance with a width of ∼100 Hz) and pulsed field gradients. ^{1}H−^{1}H correlation double-quantum filtered correlated spectroscopy (DQF-COSY) experiments were recorded over the same spectral window using 2048 complex points and sampling each of the 512 increments with 64 scans. The same acquisition parameters have been applied, together with a mixing time of 80 ms (MLEV-17 spin-lock scheme), for the acquisition of total correlation spectroscopy (TOCSY). The nuclear Overhauser effect spectroscopy (NOESY) was recorded with the same acquisition parameters and a mixing time of either 50 or 100 ms. The ^{1}H−^{13}C correlation heteronuclear single quantum coherence (HSQC) spectra were collected using a spectral window of 6.5 and 18 kHz for ^{1}H and ^{13}C respectively, and sampling each of the 512 increments with 128 scans. Further TOCSY experiments were performed after the addition of $MnCl_2$ at a final concentration of 0.1 mM. The presence of the paramagnetic ion Mn^{2+} in the solvent leads to a strong enhancement of both the longitudinal and the transversal relaxation rate of the nuclei exposed to water with resultant intensity loss of the corresponding cross-peaks. This effect is distance (and concentration) dependent so that the resonances will be progressively less affected as much as the nuclei are buried in the micelle. In practice, the intensity variation of the H_N−H_α cross-peaks was monitored by calculating the ratio between the TOCSY acquired in the presence and in the absence of the paramagnetic ions.

NMR-Based Structure Calculation. The 3D structure of plasticin-L1, either in DPC or DPC/SDS micelles, was determined using a simulated annealing protocol through the Dynamo software (http://spin.niddk.nih.gov/NMRPipe/dynamo/). Only unambiguous NOEs and $^3J_{H_NH_\alpha}$ coupling constants were used as interproton distances and Φ backbone angles were used as restraint parameters. On the basis of the relative intensity of the cross-peaks in the NOESY spectra, NOEs have been classified as strong, medium, and weak, and upper limits of 0.27, 0.33, and 0.50 nm, respectively, have been applied to restraint the corresponding interprotons distance. The potential energy was zero below the upper limit, while a harmonic potential was applied above. $^3J_{H_NH_\alpha}$ coupling constants were obtained from the one-dimensional ^{1}H spectra and/or from the DQF-COSY. The Karplus equation was used to describe the relationship between the J-coupling constant and the Φ backbone angle:

$$^3J_{H_NH_\alpha} = A\cos^2\theta + B\cos\theta + C \quad (1)$$

where $\theta = \Phi - 60°$, $A = 7.13$, $B = -1.31$, and $C = 1.56$.[18] In addition, the chemical shift values of $^1H_\alpha$, $^1H_\beta$, $^{13}C_\alpha$, and $^{13}C_\beta$ were analyzed through the software TALOS+[19] in comparison to its high-resolution structural database, to obtain both the Φ and Ψ backbone angle restraints. Only the predictions ranked as "good" were used. One thousand structures were calculated, and the 100 conformers with the lowest potential energy were selected for use in the analyses. Neither detergents nor water molecules were present during these calculations. The selected 100 conformers were aligned, and the root-mean-square deviation (RMSD) of the backbone heavy atoms was calculated with respect to the average structure. The conformer with the lowest RMSD was chosen as the starting configuration for further structural refinement through MD simulations.

dx.doi.org/10.1021/bi4008287 | *Biochemistry* 2013, 52, 7231−7241

Molecular Dynamics Simulations. MD simulations were performed with the GROMACS package[20] on plasticin-L1, in the presence of either one DPC or DPC/SDS 1:1 micelle. The GROMOS-53A6 force field[21] was used for the peptide, and the SPC model[22] was used for water. Force-field parameters and the relaxed configuration of the DPC micelle[23] were downloaded from the Internet at http://moose.bio.ucalgary.ca/. The same starting configuration was used to prepare the DPC/SDS mixed micelle (among a total of 54 DPC molecules, half of them were randomly selected and transformed into SDS). Force-field parameters for the SDS molecule[24] were downloaded from the Internet at http://www.softsimu.net/. Before the introduction of the peptide into the simulation box, the micelle has been solvated in a cubic box with edges of 8 nm. About 16 000 water molecules were used, together with 27 Na^+ ions in the case of the mixed micelle, to neutralize system total charge. One thousand steps of energy minimization were performed using the steepest descent algorithm. Then, positional restraints were applied on the heavy atoms for 100 ps to allow solvent relaxation. Finally, 10 ns equilibration was performed. After the solvent and ions had been removed from the simulation box, one plasticin-L1 molecule was placed at ~3 nm from the micelle surface with a random orientation. The starting configuration for the peptide, in each of the two cases investigated, was obtained through the NMR-based structure calculations. Water molecules and counterions have been placed in the simulation box and 1000 steps of energy minimization were performed using the steepest descent algorithm. Positional restraints were then applied on the heavy atoms for 100 ps. Finally, experimentally derived NMR restraints were introduced in the system topology. In particular, because α and β hydrogens are not explicitly present in the united-atom force field used, H_α–H_N and H_β–H_N NOE-based interproton restraints were elongated by 0.1 nm and applied on the corresponding C_α–H_N and C_β–H_N distances. Torsional restraints did not require any adjustments. One nanosecond equilibration was then performed, followed by a 100 ns production run. The simulation time step was 2 fs, and system coordinates were recorded every 4 ps. All simulations were carried out in the NPT ensemble at 300 K and 1 bar. The velocity-rescale algorithm,[25] with τ_T = 1.0 ps, was used for temperature coupling. The Berendsen[26] and Parrinello–Rahman[27,28] algorithms, with τ_P = 1.0 ps, were used for pressure coupling during the equilibration and production run, respectively. A twin-range cutoff (1.0 and 1.4 nm) was used to calculate Lennard-Jones nonbonded interactions. The particle mesh Ewald (PME) summation was used for the electrostatics with a 1.0 nm cutoff.

Measurement of Cytokine Release. Effects of stimulation by plasticin-L1 on cytokine production by peritoneal macrophages from BALB/c and C57BL/6 mice (4–5 animals per group) were determined using previously described methodologies.[7,29] The peritoneal cavity was washed with 5 mL of phosphate buffered saline, pH 7.4. Cells were placed on glass Petri dishes and nonadherent cells were discarded after 2 h of incubation at 37 °C. Adherent cells were recovered by vigorous washing with ice-cold medium. This population contained more than 95% of F4/80 positive macrophages. The peptide (20 μg/mL) was incubated with peritoneal macrophages (2×10^5 cell/well), with and without lipopolysaccharide (LPS) from *E. coli* 055:B5 (0.5 μg/mL). Cells were cultured for 24h at 37 °C in supplemented culture medium (RPMI 1640 containing 10% autologous serum, 2 mM L-glutamine, 100 IU/mL penicillin G, and 100 μg/mL streptomycin) in a humidified atmosphere of 5% CO_2 and 95% air. Cell number and viability were determined using trypan blue exclusion (>95% viable). After incubation, cells were centrifuged and supernatants were collected and kept at −20 °C until time of assay. Concentrations of tumor necrosis factor-α (TNF-α), interleukins IL-1β, IL-6, IL-10, IL-12, and IL-23 were determined in triplicate using ELISA assay kits from R&D Systems (Minneapolis, MN, USA) according to manufacturer's recommended protocols. Data are presented as mean ± standard error of the mean (SEM).

Statistical Analysis. Statistical analyses for the measurement of cytokine release were performed using commercially available software (SPSS version 13.0; SPSS Inc., Chicago, IL, USA). Data distributions were evaluated for normality using the Kolmogorov–Smirnov test and then retested with the Chi-Square test. Comparison of quantitative parametric data between two study groups was done by application of the unpaired *t*-test. Differences between the paired data were evaluated using the paired *t*-test. A *P*-value <0.05, from two-tailed tests, was considered statistically significant.

RESULTS

NMR Analysis and Structure Calculation. Figure 1 shows the hydropathicity plot[14] for plasticin-L1. Both the N-terminal (residues 1–12) and C-terminal (residue 19–25) regions of the peptide are characterized by a pattern of alternating hydrophobic and hydrophilic residues, which is compatible with an amphipathic helical folding, whereas the central domain is more hydrophilic. Table S1 (Supporting Information) shows the NMR chemical shifts and $^3J_{H_NH_\alpha}$ coupling constants for plasticin-L1 in the presence of micelles formed by either DPC or DPC/SDS. On the basis of the

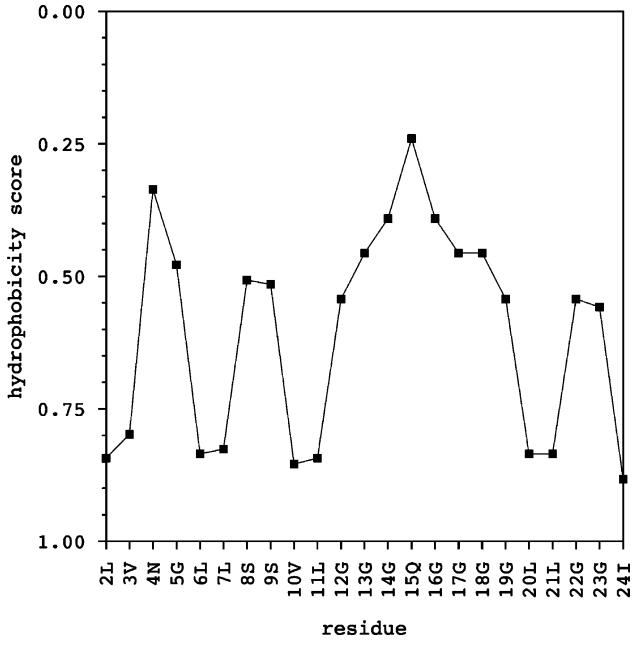

Figure 1. Hydropathicity plot obtained with method of Kyte and Doolittle,[14] with scores normalized on scale between 0 and 1. The higher the score, the higher the residue hydrophobicity. The *y*-axis has been reversed to make this profile directly comparable to those obtained from MD simulations (Figures 5 and 6).

dx.doi.org/10.1021/bi4008287 | *Biochemistry* 2013, 52, 7231–7241

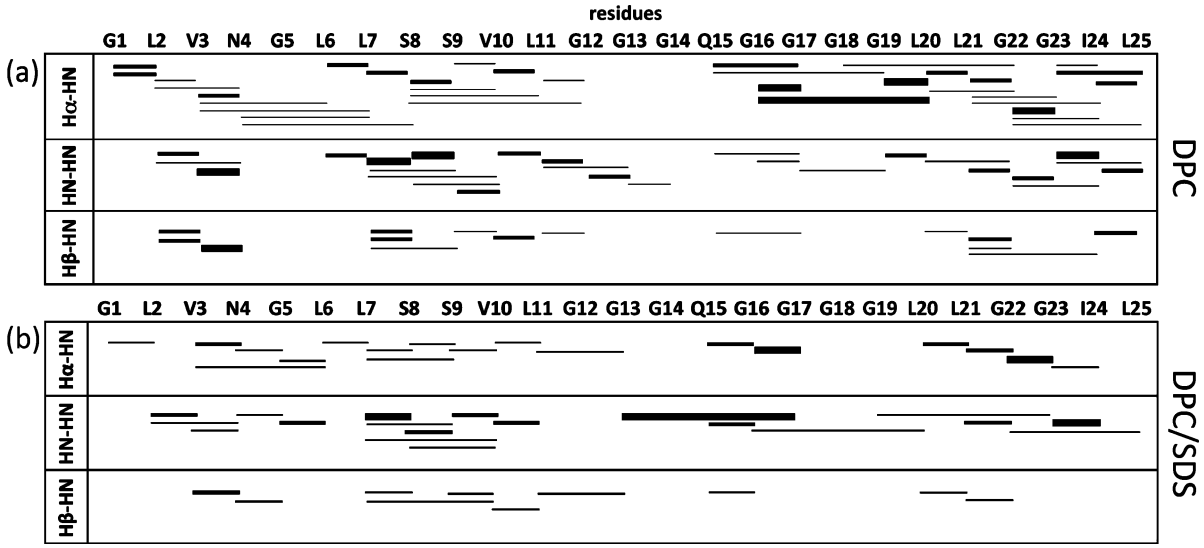

Figure 2. Short and medium-range interproton NOEs found for plasticin-L1 in presence of either (a) DPC or (b) DPC/SDS 1:1 mol/mol micelles. Each are reported as lines connecting the two residues involved. The thickness of the lines is proportional to the relative intensity of the corresponding NOESY cross-peak.

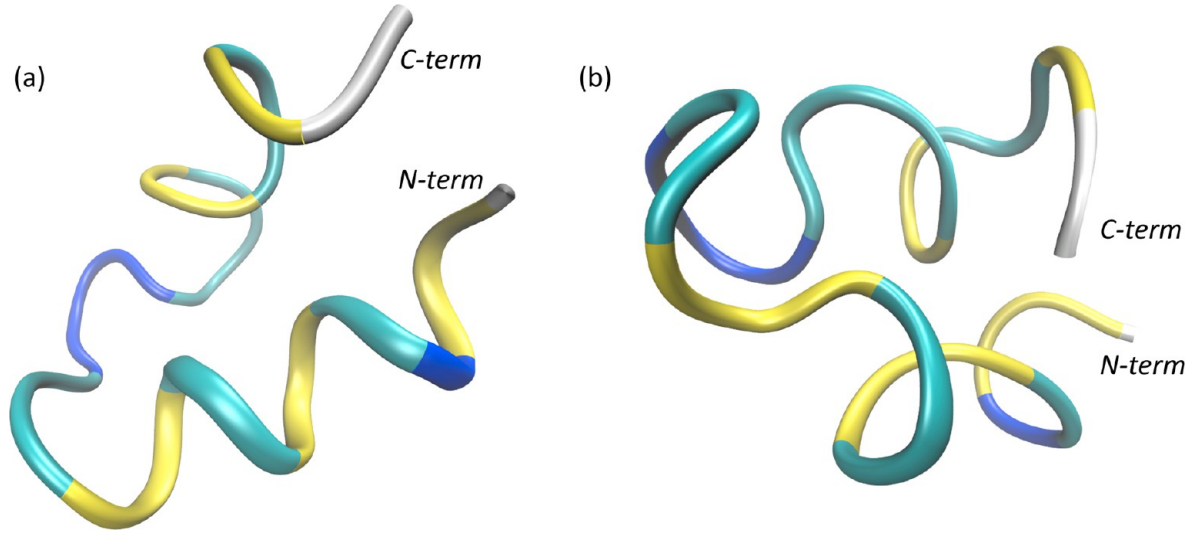

Figure 3. NMR-based structure of plasticin-L1 in presence of either (a) DPC or (b) DPC/SDS 1:1 mol/mol micelles. This is the minimum backbone RMSD structure obtained among the 100 conformers with the lowest potential energy. For the sake of clarity, only the backbone trace is shown without side chain residues. Amino acid residues are differently colored on the basis of their hydropathicity score (Figure 1): markedly hydrophilic (blue), weakly hydrophilic (cyan), and hydrophobic (yellow).

experimental chemical shifts, the application of the software TALOS+[19] results in the prediction of a helical conformation for both the N-terminal and C-terminal peptide domains, separated by an unstructured loop. In both micelle environments, a helical conformation is predicted for the region between residues 2 and 11, and between residues 20 and 22. The only exceptions were residue G5, in both the cases, and G22 in DPC/SDS whose backbone angles are not predicted with a sufficiently high consensus and so were not included in the successive structure calculations. Figure S1 (Supporting Information shows the Φ and Ψ angles obtained with TALOS +, together with their uncertainties, on the Ramachandran plot. Only the high-consensus predictions are shown. Results obtained in the two cases are comparable, although, in DPC, the points are less dispersed and the uncertainties are slightly smaller than in DPC/SDS, suggesting that the two helical domains are more defined and stable in DPC. Figure 2 shows schematically the sequential $^{1}H-^{1}H$ NOE through-space connections observed for plasticin-L1 in the two membrane-mimetic environments. Lines of different thickness are used to indicate strong, medium and weak NOEs. The total number of dipolar interprotons interactions is higher in DPC than in DPC/SDS. Moreover, the number of strong NOEs is higher in DPC and a larger number of H_i-H_{i+3} and H_i-H_{i+4} interactions are also observed. This is consistent with the conformation based upon TALOS+ predictions and the hydropathicity plot: two distinct helices at the N- and C-terminal regions of the peptide separated by an unstructured loop wherein the highest number of glycines is localized. However, in light of the lower number of NOEs observed in DPC/SDS, both helical domains are predicted to have a higher conformational plasticity with the C-terminal domain showing the greater plasticity. Figure 3

dx.doi.org/10.1021/bi4008287 | *Biochemistry* 2013, 52, 7231−7241

shows the peptide structure obtained through the DYNAMO simulated annealing procedure applied with the NMR-derived geometrical restraints. The two helical segments are evident in both the structures, either in the presence of DPC (Figure 3a) or DPC/SDS (Figure 3b) micelles. However, in DPC, the N-terminal domain comprises a regular and straight α-helix whereas the C-terminal helix is slightly distorted. As expected, the conformation obtained in the presence of the mixed micelles is even less regular: a distorted helix is clearly observed for the N-terminal segment, whereas the helical coil at the C-terminus is extremely loose.

In the case of DPC micelles, the backbone RMSD calculated from the average structure for the 100 conformers with the lowest potential energy ranges between 0.2 and 0.4 nm. The analyses show that this quite high deviation between the selected conformers is not due to poor secondary structure definition but to a rather difficult structural alignment. All the conformers are comparable to that shown in Figure 3, the high RMSD arising from the extremely variable conformation of the unfolded loop between the two helical segments and, in turn, their relative orientation. The situation in the case of DPC/SDS micelles is the same. The RMSD range is even larger (0.25–0.55 nm), because the secondary structure of the C-terminal segment is not as well-defined as in the presence of DPC micelles. Further TOCSY experiments were performed using Mn^{2+} as a paramagnetic probe. The relaxation enhancement, produced by this paramagnetic ion in the solvent, was followed for each of the amino acid residues by monitoring the intensity loss of the corresponding H_N–H_α TOCSY cross-peaks. This method has been employed previously.[30] Because the paramagnetic relaxation enhancement is distance (and concentration) dependent, it allows differentiation between residues exposed to the solvent and those buried in the micelle, thus providing information about peptide orientation and insertion into the surface of the micelle. Figure 4 shows the resulting profile for both micelle environments, where the *y*-axis has been reversed to make these results directly comparable with the distance profiles obtained from MD simulations in the Analysis of MD Simulations section. Plasticin-L1 is located at the micelle/water interface in both the cases, because the residual intensity profile oscillated throughout the peptide sequence. No completely buried regions are observed, and only the last four residues are exposed to the solvent. The alternating profile observed for the N-terminal domain of the peptide strongly supports the aforementioned helical folding, with the most hydrophobic residues interacting with the tails of the detergent molecules, whereas the hydrophilic residues are directed toward the solvent and are probably embedded within the head groups of the detergents. Similarly, the C-terminal region is characterized by an alternating pattern in the case of DPC, supporting the helical conformation found with DYNAMO. In the presence of DPC/SDS, on the other hand, a flat profile is observed in this region, which is compatible with a less rigid conformation. However, in this case, the C-terminal segment and the central loop appear to be more buried than observed in the presence of DPC micelles.

Analysis of MD Simulations. Because DYNAMO simulated annealing was applied in vacuo, we performed further structural analysis through MD simulations, using explicit solvent and detergent micelles, to complement the NMR data and characterize better the three-dimensional (3D) structure adopted by the peptide when interacting with the micelles. The radial distribution function (RDF) has been

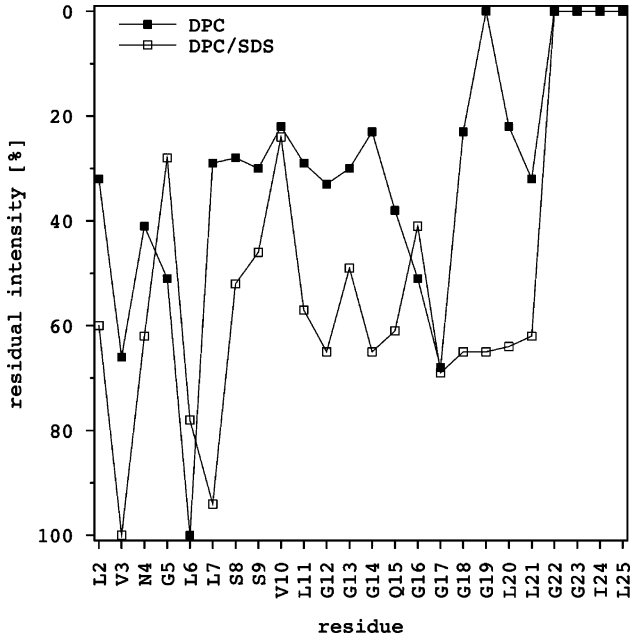

Figure 4. Residual intensity of the TOCSY cross-peaks in the H_N–H_α region, calculated as the ratio between data acquired in the presence and absence of Mn^{2+} 0.1 mM. The *y*-axis has been reversed to make this profile directly comparable to those obtained from MD simulations (Figures 5 and 6).

computed for different chemical groups of both detergents with respect to the center of mass of the micelle. RDFs have been separately calculated for the micelle equilibration stage in the absence of peptide and the production run in the presence of plasticin-L1. No significant differences are observed. Figure S2 (Supporting Information) shows the results for both micelles. For DPC, the RDF profile and time averaged radius of gyration (1.66 nm) are comparable to those previously reported.[23] On the other hand, there are no reports for mixed DPC/SDS micelles. The RDF profile and radius of gyration (1.59 nm) are comparable to those obtained for DPC micelles. This is in agreement with a study in which the hydrodynamic diameter of mixed DPC/SDS micelles has been measured with dynamic light scattering and no significant variations have been observed by varying their composition.[15]

In the presence of DPC micelles, a stable α-helix is found encompassing residues 1–11, an unstructured loop from residue 12 to 18, and a more flexible helical conformation for the C-terminal region. The C-terminal domain changes often from the α- to the π- and the 3_{10}-helices, although the former was the predominant motif. As expected, the backbone RMSD spans about 0.3 nm, indicating that the peptide adopts different conformations along the MD, whose difference is due mostly to the central unfolded loop and the relative orientation of the two helical fragments. A cluster analysis was performed with the Gromos method[31] using a 0.1 nm cutoff. Only four clusters were found to have an occurrence larger than 5% of total simulation time, altogether accounting for 80% of conformers. However, the peptide was not found to adopt the corresponding conformations "randomly". A closer inspection revealed that each of the main clusters pertained to a specific temporal window of the simulation, thus allowing sampling in successive steps and ascertaining how the folded (restrained) peptide relaxed upon interaction with the micelle. It is important to stress that the folding process itself was not

dx.doi.org/10.1021/bi4008287 | *Biochemistry* 2013, 52, 7231–7241

investigated; MD was used to refine the equilibrium 3D structure obtained on the basis of NMR results. From our current data, we cannot state whether folding is completed prior to or after peptide binding to the micelle.

For each central conformer of the clusters, side- and top-view images were created to show a 3D representation of the system. In addition, a plot of the distance between the center of mass of the amino acid residues and that of the micelle was produced to provide a quantitative comparison of the insertion depth of the different regions of the peptide. Only the figures showing the final equilibrium conformation have been included in the main article, whereas the others are available in the Supporting Information. During the starting equilibration stage, the peptide approaches and starts to interact with the surface of the DPC micelle (Figure S3a–c, Supporting Information). The first residues to bind the micelle are V10 and L11, which are the most hydrophobic according to the hydropathicity plot (Figure 1). The N-terminal and C-terminal helices are almost parallel. During the first ∼2 ns of the production run, the entire N-terminal helix resides on the micelle's surface, inserted between DPC head groups and rotated along its main axis. Finally, (Figure S3d–f, Supporting Information) the peptide inserts into the micelle with the hydrophobic residues directed toward the interior. The global peptide conformation does not change significantly, with the two helical segments remaining parallel. The C-terminal domain, which "followed" the other helix during its rotation, is still exposed to the solvent. At ∼10 ns, the C-terminal helix starts to rotate with respect to the N-terminal domain. At ∼20 ns this movement ends, with the C-terminal helix still exposed to water but now facing a free area of the micelle surface (Figure S3g–i, Supporting Information). At ∼40 ns, the C-terminal helix inserts with its hydrophobic residues pointing toward the DPC hydrophobic tails (Figure S3j–l, Supporting Information). The N-terminal helix is also embedded within the head group of the detergent but is slightly displaced. Both helices are inserted at the same depth and are located at the micelle/water interface. Finally, at ∼60 ns, plasticin-L1 finds its equilibrium conformation, which does not change further up to the end of the simulation (Figure 5). This conformation is characterized by a helix–loop–helix super-secondary motif approximating to a "V". Both helices are localized at the micelle/water interface, with the N-terminal helix being slightly more buried than the other. As expected, the hydrophilic central loop never inserts into the micelle.

In the presence of DPC/SDS micelles, a stable α-helix is found encompassing residues (1–11) as in the case of DPC micelles. However, the central unfolded portion of the peptide is two residues longer (i.e., from residue 12 to 20). As a consequence, only one helical turn is observed at the C-terminal region. As expected from NMR results, backbone RMSD spans a larger interval, about 0.5 nm instead of 0.3 nm, indicating that overall conformation of the peptide is more unstable in DPC/SDS. A cluster analysis was performed with the same parameters used for DPC simulation. Again, only four clusters are found with a frequency larger than 5% of total simulation time, but they account for only 50% of the conformers. In contrast to the DPC model, the starting equilibration stage was not sufficient to observe any peptide–micelle close-contact interaction. After ∼7.6 ns of the production run, the peptide binds to the micelle surface with the N-terminus first approaching the micelle (Figure S4a–c, Supporting Information). The peptide takes another ∼1.5 ns to lie on the micelle surface with a helix–loop–helix super-

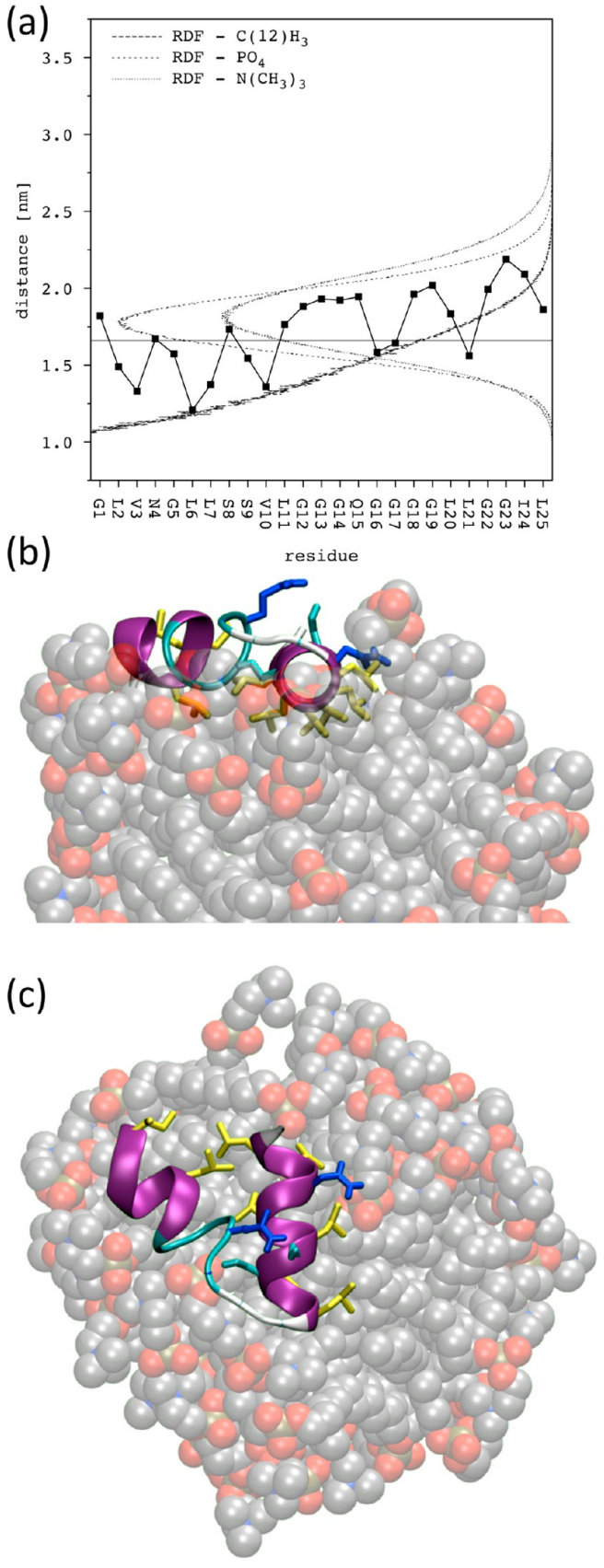

Figure 5. Central structure of main peptide conformation cluster among 100 ns MD simulation in presence of DPC micelles. This cluster pertains to simulation time from ∼60 to 100 ns. (a) The residues center of mass distance (time averaged) from the center of mass of the micelle is shown (filled squares). The solid horizontal line

dx.doi.org/10.1021/bi4008287 | Biochemistry 2013, 52, 7231–7241

Figure 5. continued

is reported as a reference for the radius of gyration of the micelle. The differently dashed curves are the radial distribution functions obtained for three different chemical groups of DPC. The corresponding 3D side- and top-views are shown in (b) and (c), respectively, where residues are differently colored according to their hydropathicity scores (Figure 1): markedly hydrophilic (blue), weakly hydrophilic (cyan), and hydrophobic (yellow).

secondary motif, arranged in an "L" conformation (Figure S4d–f, Supporting Information). During the rest of the simulation, plasticin-L1 slowly orientates between detergent head groups but is always localized at the micelle/water interface, as in the case of DPC. In the 29–53 ns interval, the corresponding cluster is characterized by an "extended" conformation, with the two helices lying almost on the same line (Figure S4g–i, Supporting Information). This alignment is then lost in the subsequent main cluster (Figure S4j–l, Supporting Information) over the 59–76 ns temporal window. Finally, the most populated conformation is reached (Figure 6), characterized by an "L" global shape. This is the main difference with respect to the equilibrium conformation obtained in DPC micelles, whereas the global insertion depth is comparable in the two membrane models.

In DPC, the most hydrophilic residue Q15 is always observed to interact with water, whereas in the case of DPC/SDS, Q15 strongly interacts with the sulfate head groups of SDS, often forming H-bonds. In DPC, (Q15)–N_δ–H···O–PO_3(DPC) H-bonds are found with a frequency of 21% relative to total simulation time. However, these interactions between peptide and detergent head groups were observed only during the first 30 ns, suggesting that they are important during the initial stage of peptide binding but, as soon as the equilibrium conformation is reached, Q15 preferentially interacts with water molecules. In DPC/SDS, (Q15)–N_δ–H···O–PO_3(DPC) H-bonds have a frequency of only 7% and, again, are observed only during the initial stage of binding. On the other hand, the occurrence of (Q15)–N_δ–H···O–SO_3(SDS) H-bonds was 38% of total simulation time and, most importantly, these interactions were observed throughout the simulation. This stronger interaction between Q15 and the sulfate head groups forces the central unfolded loop to "adhere" to the surface of the mixed micelle. This is compatible with the NMR paramagnetic relaxation enhancement experiments (Figure 4), where the central peptide portion is less exposed to the solvent than observed in DPC. This might also explain the different peptide global shape observed. In the DPC micelle, the flexible loop is not "anchored" to micelle surface, allowing for the two helices to come closer to each other and to form a more compact V conformation.

Effects of Plasticin-L1 on Release of Cytokines. Release of the proinflammatory cytokine IL-1β from unstimulated peritoneal macrophages from both C57BL/6 and BALB/C mice was significantly ($P < 0.05$) increased by incubation with plasticin-L1 (20 μg/mL; approximately 9 μM). The peptide also potentiated the stimulation produced by lipopolysaccharide (LPS), but the effect was not significant (Figure 7). Incubation with plasticin-L1 (20 μg/mL) also increased release of the proinflammatory cytokines IL-23 from both BALB/C and C57BL/6 mice and TNF-α from C57BL/6 mice. The effect was significant ($P < 0.05$) for the unstimulated macrophages only (Figure 7). Treatment with the peptide

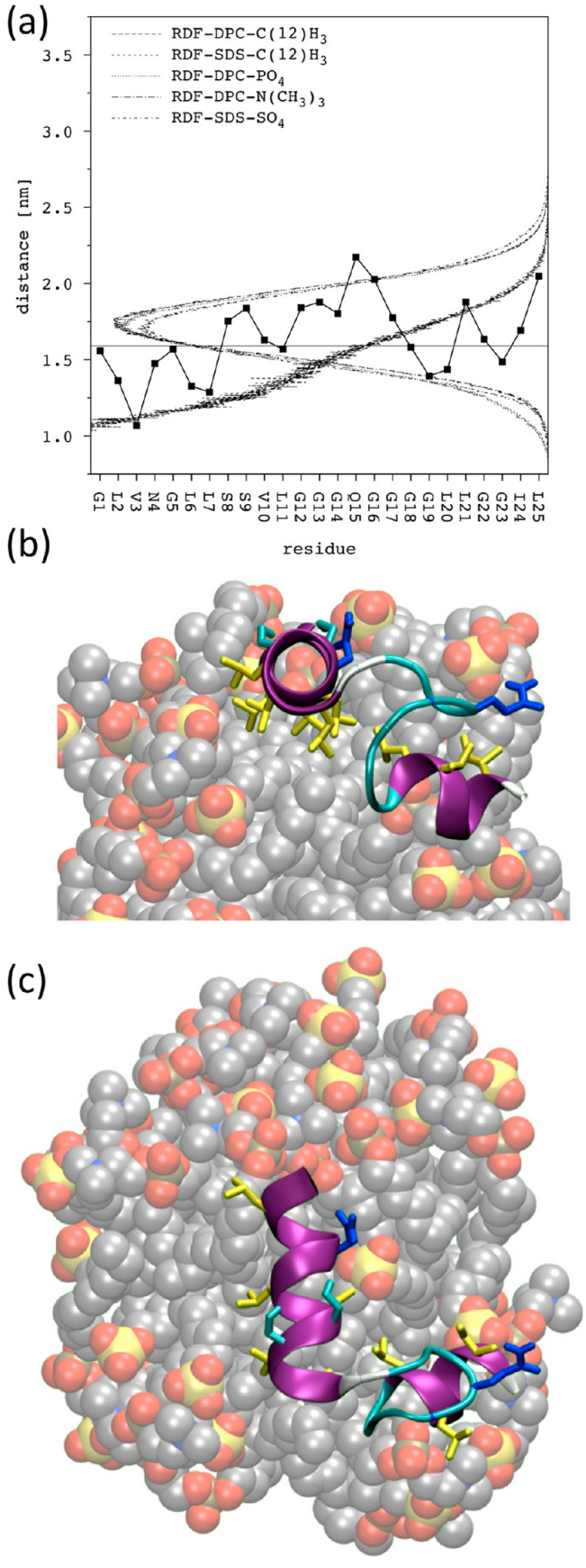

Figure 6. Central structure of the main peptide conformation cluster among 100 ns MD simulation in the presence of DPC/SDS 1:1 mixed micelles. This cluster pertains to simulation time from ~77 to 100 ns.

dx.doi.org/10.1021/bi4008287 | *Biochemistry* 2013, 52, 7231–7241

Figure 6. continued

(a) The residues center of mass distance (time averaged) from the center of mass of the micelle is shown (filled squares). The solid horizontal line is reported as a reference for the radius of gyration of the micelle. The differently dashed curves are the radial distribution functions obtained for different chemical groups of DPC and SDS. The corresponding 3D side- and top-views are shown in (b) and (c), respectively, where residues are differently colored according to their hydropathicity scores (Figure 1): markedly hydrophilic (blue), weakly hydrophilic (cyan), and hydrophobic (yellow).

significantly ($P < 0.05$) increased release of the proinflammatory cytokine IL-12 from unstimulated macrophages from both C57BL/6 and BALB/C mice (Figure 7). Release of IL-6 from both unstimulated ($P < 0.01$) and LPS-stimulated ($P < 0.01$) macrophages from BALB/C mice was significantly increased in the presence of plasticin-L1 (20 μg/mL). In the case of macrophages from C57BL/6 mice, the effect was significant ($P < 0.01$) only for unstimulated cells (Figure 7). Lower doses (1 and 10 μg/mL) did not induce any significant change in cytokine production (data not shown). Treatment with plasticin-L1 (20 μg/mL) had no significant effect on the release of the anti-inflammatory cytokine IL-10 from either unstimulated or LPS-stimulated cells (data not shown).

DISCUSSION

Analysis of the structural properties of plasticin-L1 provided in this study has revealed a marked affinity of the peptide for both neutral and anionic membrane models. Plasticin-L1 is not sufficiently soluble in water, methanol, TFE/water, and chloroform to permit conformational analysis in these isotropic solvents. However, plasticin-L1 is very soluble in micellar media (either DPC or DPC/SDS), allowing for an in-depth NMR structural investigation of the 3D structure adopted when the peptide is bound to these models of the cell membrane. The experimentally derived NMR geometrical restraints were used to determine the most energetically favorable conformation in vacuo. The same restraints were then applied in an explicit solvent and micelle simulation. The final equilibrium structure was found to be located at the micelle/water interface in both DPC and DPC/SDS, and its insertion depth and orientation with respect to the micelle surface resulted to be comparable and in agreement with the NMR paramagnetic enhanced relaxation experiments. As plasticin-L1 is a highly hydrophobic peptide, the main driving force for its interaction with the micelles is the need to minimize contacts with water. At the same time, the presence of hydrophilic residues throughout the molecule allows the peptide to fold in a global amphipathic 3D structure at the membrane/water interface. The hydrophobic residues interact with the nonpolar tails of the detergent molecules and the hydrophilic residues interact with water and the polar head groups. In particular, the alternate pattern of two hydrophilic and two hydrophobic residues in the N-terminal domain (residues 1−11) leads to a very stable α-helical conformation. In the C-terminal region, the same alternate pattern of hydrophobic/hydrophilic amino acids is present but involves fewer residues, leading to a more conformationally mobile helix. The presence of multiple glycines in the central and C-terminal regions makes these domains less amphipathic than the N-terminal helix. The central region of plasticin-L1 is characterized by a relatively long, glycine rich, markedly hydrophilic and unstructured loop. Its conformational plasticity endows the peptide with the possibility of adopting multiple overall conformations with different relative orientations of the two helical domains. In both DPC and DPC/SDS micelles, the most hydrophilic residue Q15, located in the middle of the central loop, establishes H-bonding interactions with detergent head groups. However, although H-bonds were observed with SDS throughout the MD simulation, those that formed with DPC were present only during the initial stage of peptide/micelle binding. As a consequence, Q15 has a strong interaction with SDS head groups despite its lack of net positive charge. In the case of mixed micelles, the central loop is forced to stay closer to surface of the micelle than in the case of DPC. Thus, although a more "extended" helix−loop−helix supersecondary structure is found in mixed DPC/SDS micelles, a more compact V conformation is observed in the case of DPC.

Earlier circular dichroism studies indicated marked solvent dependent malleability with plasticin-L1 adopting a disordered or random coil conformation in water but a well-defined β-sheet structure in methanol and a helical structure in 50% TFE−water.[9] The peptide concentration required for NMR characterization (mM range) is much higher than that required for circular dichroism (μM range) precluding investigations in these solvents, due to poor peptide solubility. Nevertheless, our observation of the formation of α-helical domains upon interaction with detergent micelles is consistent with conformational data recorded when the peptide was dissolved in TFE−water mixtures,[9] the only solvent system employed in circular dichroism studies that can be considered to reproduce a membrane-like environment.[32]

The observed lack of antimicrobial activity of plasticin-L1 is consistent with the absence of a net positive charge at neutral pH, the general correlation between the cationic character of peptides and their affinity toward prokaryotic membranes being quite well understood.[33] However, a structurally related neutral glycine/leucine-rich peptide, named leptoglycin, was isolated from skin secretions of a frog from the same genus, *Leptodactylus pentadactylus*, and shown to inhibit the growth of the Gram-negative pathogen *Pseudomonas aeruginosa*, while being inactive against Gram-positive bacteria and fungi and not hemolytic.[34]

The study has demonstrated that incubation with plasticin-L1 (20 μg/mL) has a stimulatory effect on the release of proinflammatory cytokines from mouse peritoneal macrophages. Proinflammatory cytokines function as immunostimulatory agents and the important immunomodulatory role played by peptides at the interface between innate and adaptive immunity is becoming appreciated.[8,35] Most studies to-date have focused on cationic peptides such as cathelicidins (LL-37) and defensins, revealing a complex mix of immune regulatory activities mediated through a host of mechanisms that involve various receptors, signaling pathways and transcription factors.[36] These include stimulation of chemokine production, inhibition/induction of both pro- and anti-inflammatory cytokines, LPS neutralization, mast cell degranulation and chemotaxis of various leukocytes.

We have recently isolated a structurally unrelated neutral peptide, named frenatin-2D, from norepinephrine-stimulated skin secretions of the Tyrrhenian painted frog *Discoglossus sardus* that was devoid of antimicrobial activity but altered cytokines production by mouse peritoneal macrophages in a manner similar (but not identical) to that observed for plasticin-L1.[7] In particular, treatment with frenatin-2D significantly stimulated production of TNF-α and IL-1β by

dx.doi.org/10.1021/bi4008287 | *Biochemistry* 2013, 52, 7231−7241

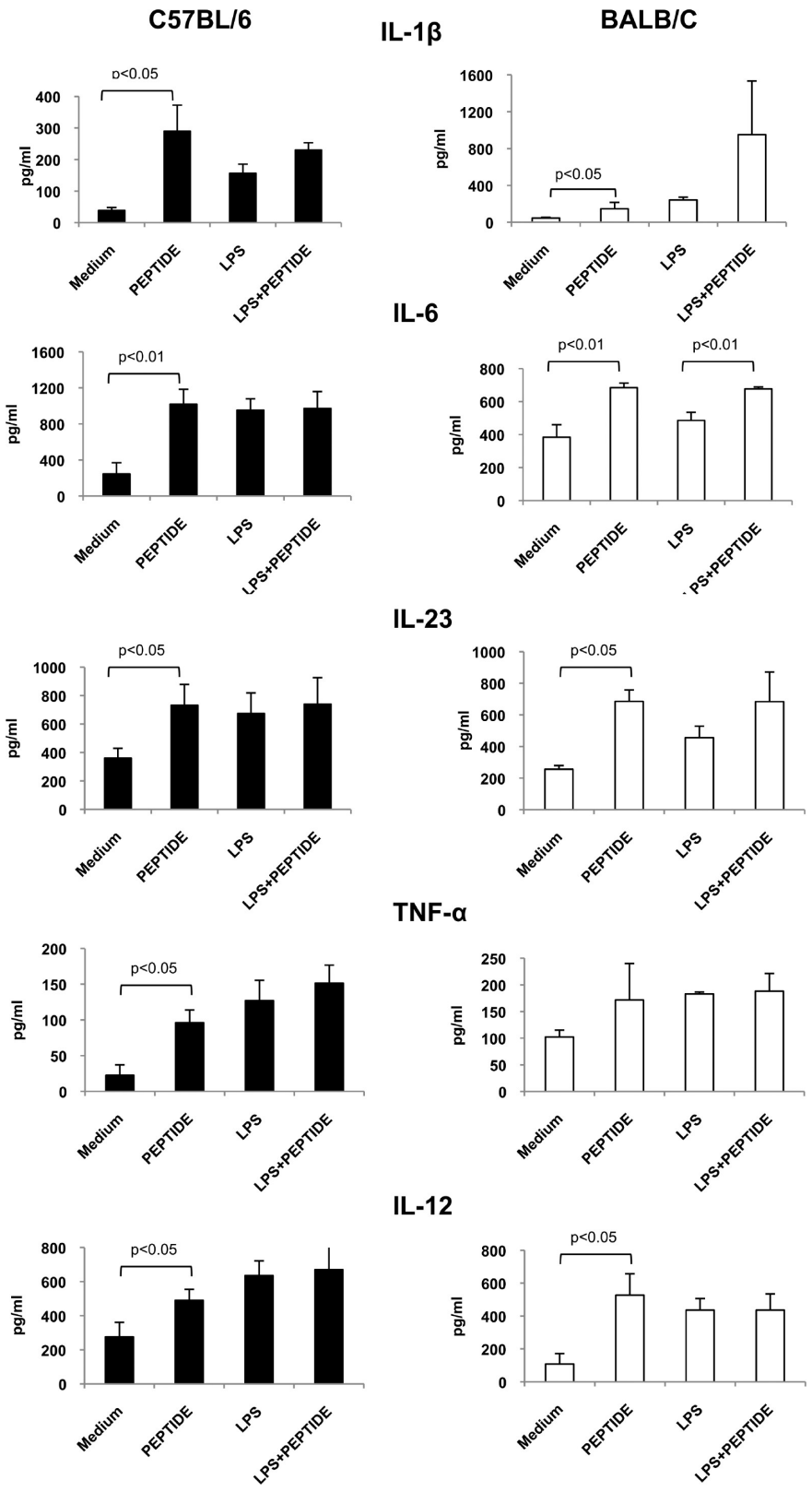

Figure 7. Effects of incubation with plasticin-L1 (20 μg/mL) on production of proinflammatory cytokines by unstimulated and LPS-stimulated peritoneal macrophages from C57BL/6 and BALB/C mice. Medium refers to incubation with medium only.

macrophages but the peptide did not potentiate the stimulation produced by LPS. The peptide also increased IL-12 production in both unstimulated and LPS-stimulated cells, but stimulatory effects on IL-6 production were not significant.[7] In present study, plasticin-L1 enhanced the production of all proinflammatory cytokines tested in macrophage cultures derived from C57BL/6 mice. In Th-2 type BALB/C mice, there was no significant increase in TNF-α production (Figure 7). In all the cases, there was no significant effect on the production of proinflammatory cytokines by LPS-stimulated macrophages. It

dx.doi.org/10.1021/bi4008287 | *Biochemistry* 2013, 52, 7231−7241

is improbable that plasticin-L1 binds to the LPS receptor as the effects of LPS on cytokine production were the same whether the peptide was present during 24 h of incubation with LPS (Figure 7) or preincubated with cells for 2 h, removed by washing, followed by incubation with LPS (data not shown).

The data raise the possibility that a fairly general mechanism exists whereby these neutral peptides act on macrophages in frog skin to produce a cytokine-mediated stimulation of innate and/or adaptive immunity, thus protecting the animal against invading microorganisms.

It is not known whether stimulation of cytokine production by plasticin-L1 arises from a nonspecific interaction of the peptide with the macrophage membrane or from interaction with a specific receptor. The plasticin-L1 sequence contains three GXXXG motif repeats (where X denotes any amino acid), suggesting that the peptide may fold as a trans-membrane helix and possibly oligomerize into bundles. Indeed, GXXXG is the most common structural motif found at the interface between interacting trans-membrane helices. However, Leu, Val, and Ile are most commonly found in the GXXXG motif, and the presence of these hydrophobic residues ensures high affinity for the hydrophobic inner membrane region while the small (and weakly hydrophilic) glycines make insertion easier and facilitate different trans-membrane helices to come into close contact and assemble into bundles.[37,38] In plasticin-L1, the GXXXG motifs in the central and C-terminal regions contain additional glycines probably making the peptide too hydrophilic to insert in the cell membrane. The ability of plasticin-L1 to oligomerize will be addressed in future work.

Although generation of high levels of pro-inflammatory cytokines may lead to toxicity, enhancing their selective release of through a rational optimization of peptide sequence may represent a possible therapeutic application of neutral frog skin peptides such as plasticin-L1 and frenatin-2D.[7] Proinflammatory cytokines function as immunostimulatory agents, and several compounds that stimulate cytokine release are in clinical practice.[39] The peptides may have an enhancing effect on the innate immune response to microbial infection and tumorigenesis. This scenario could be beneficial in a clinical setting in which the first line of defense should be enhanced without possible complications due to induction of autoimmunity. Further investigations are needed to elucidate the precise mechanism of action of plasticin-L1, but the present work forms the basis for a deeper understanding of structure−function relationships. In the future, the peptide may provide a template to develop a new immunomodulatory class of molecules to be used in concert with other antimicrobial and/or anticancer drugs.

■ ASSOCIATED CONTENT

Supporting Information

Additional data on the NMR and MD characterization of plasticin-L1 including resonance assignments, high-consensus predictions, radial distribution functions, and snapshots of plasticin-L1 in the presence of a DPC micelle and a DPC/SDS 1:1 mixed micelle. This material is available free of charge via the Internet at http://pubs.acs.org.

■ AUTHOR INFORMATION

Corresponding Author

*Mariano Andrea Scorciapino. Address: Department of Chemical and Geological Sciences, University of Cagliari, Cittadella Universitaria di Monserrato, SS554 bivio Sestu, I-09042, Monserrato (CA), Italy. Tel: +39-070-675-4354. E-mail: scorciapino@unica.it.

Funding

Regione Autonoma della Sardegna, Italy, L.R. 7/2007 (fiscal year 2009); Ministry of Science, Belgrade, Serbia (175071, 175069, and 175103); Terry Fox fund for Cancer Research; G. Manzo's Ph.D. fellowship by Regione Autonoma della Sardegna (P.O.R. FSE 2007−2013).

Notes

The authors declare no competing financial interest.

■ ACKNOWLEDGMENTS

Dr. Lorant Janosi and Dr. Attilio Vittorio Vargiu are acknowledged for fruitful discussions about the MD simulations.

■ ABBREVIATIONS

DPC, dodecylphosphocholine; DQF-COSY, double quantum filtered correlation spectroscopy; HSQC, heteronuclear single quantum correlation spectroscopy; IL, interleukin; LPS, lipopolysaccharide; MD, molecular dynamics; NMR, nuclear magnetic resonance; NOESY, nuclear Overhauser effect spectroscopy; PME, particle mesh Ewald; RDF, radial distribution function; RMSD, root-mean-square deviation; SDS, sodium dodecylsulphate; SPC, simple point charge; TFE, trifluoroethanol; TSP, trimethylsilyl propionic acid; TNF, tumor necrosis factor; TOCSY, total correlation spectroscopy

■ REFERENCES

(1) Livermore, D. M. (2009) Has the era of untreatable infections arrived? *J. Antimicrob. Chemother. 64* (Suppl1), i29−36.

(2) Kastin, J. A., Ed. (2013) *Handbook of Biologically Active Peptides*. 2nd ed., Academic Press, San Diego, CA.

(3) Rinaldi, A. C. (2002) Antimicrobial peptides from amphibian skin: an expanding scenario. *Curr. Opin. Chem. Biol. 6*, 799−804.

(4) Conlon, J. M. (2011) The contribution of skin antimicrobial peptides to the system of innate immunity in anurans. *Cell Tissue Res. 343*, 201−212.

(5) Structural diversity and species distribution of host-defense peptides in frog skin secretions. *Cell. Mol. Life Sci. 68*, 2303−2315.

(6) Perron, G. G., Zasloff, M., and Bell, G. (2006) Experimental evolution of resistance to an antimicrobial peptide. *Proc. Biol. Sci. 273*, 251−256.

(7) Conlon, J. M., Mechkarska, M., Pantic, J. M., Lukic, M. L., Coquet, L., Leprince, J., Nielsen, P. F., and Rinaldi, A. C. (2013) An immunomodulatory peptide related to frenatin 2 from skin secretions of the Tyrrhenian painted frog *Discoglossus sardus* (Alytidae). *Peptides 40*, 65−71.

(8) Haney, E. F, and Hancock, R. B. (2013) Peptide design for antimicrobial and immunomodulatory applications. *Biopolymers*, DOI: 10.1002/bip.22250.

(9) Conlon, J. M., Abdel-Wahab, Y. H., Flatt, P. R., Leprince, J., Vaudry, H., Jouenne, T., and Condamine, E. (2009) A glycine-leucine-rich peptide structurally related to the plasticins from skin secretions of the frog *Leptodactylus laticeps* (Leptodactylidae). *Peptides 30*, 888−892.

(10) El Amri, C., and Nicolas, P. (2008) Plasticins: membrane-damaging peptides with chameleon-like properties. *Cell. Mol. Life Sci. 65*, 895−909.

(11) Jooanne, P., Falord, M., Chesneau, O., Lacombe, C., Castano, S., Desbat, B., Auvynet, C., Nicolas, P., Msadek, T., and El Amri, C. (2009) Comparative study of two plasticins: specificity, interfacial behavior, and bactericidal activity. *Biochemistry 48*, 9372−9383.

(12) Bruston, F., Lacombe, C., Zimmermann, K., Piesse, C., Nicolas, P., and El Amri, C. (2007) Structural malleability of plasticins:

preorganized conformations in solution and relevance for antimicrobial activity. *Biopolymers 86*, 42−56.
(13) Gasteiger, E., Hoogland, C., Gattiker, A., Duvaud, S., Wilkins, M. R., Appel, R. D., and Bairoch, A. (2005) *Protein identification and analysis tools on the ExPASy server*. in *The Proteomics Protocols Handbook*, Walker, J. M., Ed., Humana Press, Totowa, NJ, pp 571−607.
(14) Kyte, J., and Doolitle, R. F. (1982) A simple method for displaying the hydropathic character of a protein. *J. Mol. Biol. 157*, 105−132.
(15) Manzo, G., Carboni, M., Rinaldi, A. C., Casu, M., and Scorciapino, M. A. (2013) Characterization of sodium dodecylsulphate and dodecylphosphocholine mixed micelles through NMR and dynamic light scattering. *Magn. Reson. Chem. 51*, 176−183.
(16) Ogg, R., Kingsley, P., and Taylor, J. (1994) WET, a T1- and B1-insensitive water-suppression method for in vivo localized 1H NMR spectroscopy. *J. Magn. Reson., Ser. B 104*, 1−10.
(17) Smallcombe, S., Patt, S. L., and Keifer, P. (1995) WET solvent suppression and its applications to LC NMR and high-resolution NMR spectroscopy. *J. Magn. Reson., Ser. A 117*, 295−303.
(18) Habeck, M., Rieping, W., and Nilges, M. (2005) Bayesian estimation of Karplus parameters and torsion angles from three-bond scalar couplings constants. *J. Magn. Reson. 177*, 160−165.
(19) Shen, Y., Delaglio, F., Cornilescu, G., and Bax, A. (2009) TALOS+: A hybrid method for predicting protein backbone torsion angles from NMR chemical shifts. *J. Biomol. NMR 44*, 213−223.
(20) Hess, B., Kutzner, C., Van der Spoel, D., and Lindahl, E. (2008) GROMACS 4: Algorithms for highly efficient, load-balanced, and scalable molecular simulation. *J. Chem. Theory Comput. 4*, 435−447.
(21) Oostenbrink, C., Villa, A., Mark, A. E., and Van Gunsteren, W. F. (2004) A biomolecular force field based on the free enthalpy of hydration and solvation: The GROMOS force-field parameter sets 53A5 and 53A6. *J. Comput. Chem. 25*, 1656−1676.
(22) Berendsen, H. J. C., Postma, J. P. M., Van Gunsteren, W. F., and Hermans, J. (1981) Interaction models for water in relation to protein hydration. in *Intermolecular forces*. Pullman, B., and Reidel, D. Eds., Springer, Dordrecht, The Netherlands, pp 331−342.
(23) Tieleman, D. P., Van der Spoel, D., and Berendsen, H. J. C. (2000) Molecular dynamics simulations of dodecylphosphocholine micelles at three different aggregate sizes: micellar struture and chain relaxation. *J. Phys. Chem. B 104*, 6380−6388.
(24) Sammalkorpi, M., Karttunen, M., and Haataja, M. (2007) Structural properties of ionic detergent aggregates: a large-scale molecular dynamics study of sodium dodecyl sulphate. *J. Phys. Chem. B 111*, 11722−11733.
(25) Bussi, G., Donadio, D., and Parrinello, M. (2007) Canonical sampling through velocity rescaling. *J. Chem. Phys. 126*, 014101.
(26) Berendsen, H. J. C., Postma, J. P. M., Van Gunsteren, W. F., Di Nola, A., and Haak, J. R. (1984) Molecular dynamics with coupling to an external bath. *J. Chem. Phys. 81*, 3684−3690.
(27) Nosé, S., and Klein, M. L. (1976) Constant pressure molecular dynamics for molecular systems. *Mol. Phys. 50*, 1055−1076.
(28) Parrinello, M., and Rahman, A. (1981) Polymorphic transitions in single crystals: A new molecular dynamics method. *J. Appl. Phys. 52*, 7182−7190.
(29) Popovic, S., Urbán, E., Lukic, M., and Conlon, J. M. (2012) Peptides with antimicrobial and anti-inflammatory activities that have therapeutic potential for treatment of acne vulgaris. *Peptides 34*, 275−282.
(30) Abbassi, F., Galanth, C., Amiche, M., Saito, K., Piesse, C., Zargarian, L., Hani, K., Nicolas, P., Lequin, O., and Ladram, A. (2008) Solution structure and model membrane interactions of temporins-SH, antimicrobial peptides from amphibian skin. A NMR spectroscopy and differential scanning calorimetry study. *Biochemistry 47*, 10513−10525.
(31) Daura, X., Gademann, K., Jaun, B., Seebach, D., Van Gunsteren, W. F., and Mark, A. E. (1999) Peptide folding: when simulation meets experiment. *Ang. Chem., Int. Ed. 38*, 236−240.
(32) Scorciapino, M. A., Pirri, G., Vargiu, A. V., Ruggerone, P., Giuliani, A., Casu, M., Buerck, J., Wadhwani, P., Ulrich, A. S., and Rinaldi, A. C. (2012) A novel dendrimeric peptide with antimicrobial properties: structure-function analysis of SB056. *Biophys. J. 102*, 1039−1048.
(33) Hancock, R. E. W., and Sahl, H. G. (2006) Antimicrobial and host-defense peptides as new anti-infective therapeutic strategies. *Nat. Biotechnol. 24*, 1551−1557.
(34) Sousa, J. C., Berto, R. F., Gois, E. A., Fontenele-Cardi, N. C., Honório, J. E., Jr., Konno, K., Richardson, M., Rocha, M. F., Camargo, A. A., Pimenta, D. C., Cardi, B. A., and Carvalho, K. M. (2009) Leptoglycin: a new glycine/leucine-rich antimicrobial peptide isolated from the skin secretion of the South American frog *Leptodactylus pentadactylus* (Leptodactylidae). *Toxicon 54*, 23−32.
(35) Choi, K. Y., Chow, L. N., and Mookherjee, N. (2012) Cationic host defence peptides: multifaceted role in immune modulation and inflammation. *J. Innate Immun. 4*, 361−370.
(36) Diamond, G., Beckloff, N., Weinberg, A., and Kisich, K. O. (2009) The roles of antimicrobial peptides in innate host defense. *Curr. Pharm. Des. 15*, 2377−2392.
(37) Russ, W. P., and Engelman, D. M. (2000) The GxxxG motif: a framework for transmembrane helix-helix association. *J. Mol. Biol. 296*, 911−919.
(38) Fink, A., Sal-Man, N., Gerber, D., and Shai, Y. (2012) Transmembrane domains interactions within the membrane milieu: principles, advances and challenges. *Biochim. Biophys. Acta 1818*, 974−983.
(39) Chatzidakis, I., and Mamalaki, C. (2010) T-cells as sources and targets of TNF: implications for immunity and autoimmunity. *Curr. Dir. Autoimmun. 11*, 105−118.